STET

Characterization and Modeling of the Subsurface in the Context of Ecological Transition
Yannick Peysson and Jacques Pironon (Guest Editors)

REGULAR ARTICLE

OPEN ∂ ACCESS

Calculation of Joule–Thomson and isentropic expansion coefficients for two-phase mixtures

Ababakari Oumarou Ali, Daniel Broseta[*], and Dan Vladimir Nichita

CNRS UMR 5150, Laboratoire des Fluides Complexes et leurs Réservoirs, Université de Pau et des Pays de l'Adour, B.P. 1155, 64013 Pau Cedex, France

Abstract. Joule–Thomson (JT) and isentropic expansion coefficients describe the temperature change induced by a pressure variation under isenthalpic and isentropic conditions, respectively. They are commonly used to model a variety of processes in which either fluid compression or expansion is involved. While a lot of work has been devoted to inferring the JT coefficient from an equation of state when the fluid is a single phase, little attention has been paid to multiphase fluids, where phase equilibrium has to be taken into account; previous work has only addressed the construction on the JT inversion curve. In the present paper, we describe and implement an approach to calculate these two coefficients for multi-component fluid systems, including when they form two different phases, liquid, and vapor, in thermodynamic equilibrium. The only ingredients are an equation of state and expressions for the ideal part of the specific heats of the fluid components. We make use of cubic equations of state, but any thermodynamic model can be used in the proposed framework. Calculations conducted with typical geofluids, some of them containing CO_2, show that these coefficients are discontinuous at phase boundaries (where enthalpy and entropy variations exhibit angular points), as expected with any thermodynamic quantity built from first-order derivatives of state functions, and cannot be simply inferred from the coefficients of the liquid and vapor phases.

Keywords: Joule–Thomson coefficient, Isentropic expansion coefficient, Carbon dioxide, Inversion curve.

1 Introduction

Depending on whether the enthalpy H or entropy S of a given fluid system is kept constant, the variation of temperature induced by a pressure variation is described by, respectively, the Joule–Thomson (JT) coefficient

$$\mu_{JT} = \left(\frac{\partial T}{\partial p}\right)_H, \tag{1}$$

and the coefficient of isentropic expansion

$$\mu_S = \left(\frac{\partial T}{\partial p}\right)_S. \tag{2}$$

These coefficients are the slopes of the isenthalps (H = constant) and isentrops (S = constant) in the p–T (pressure–temperature) plane. A positive (resp. negative) value means the fluid experiences cooling (resp. heating) when submitted to depletion. As a rule, the coefficient of isentropic expansion is positive, except in rare instances, *e.g.*, liquid water at temperatures near 0 °C or liquid He^3 near 0 K [1], whereas JT coefficients commonly exhibit positive (usually for gases) or negative (for liquids and supercritical fluids) values, depending on the p and T conditions. The Joule–Thomson Inversion Curve (JTIC) in the p–T plane separates the cooling and the heating regions; it connects points where the JT coefficients are equal to zero (or where they change sign when a discontinuity arises). This curve delineates the T and p conditions where cooling occurs upon depletion ($\mu_{JT} > 0$) from conditions where heating occurs ($\mu_{JT} < 0$).

These coefficients are key for describing a variety of processes in which a variation of fluid pressure, whether a compression or an expansion, generates a change in temperature, which is either exploited or avoided, depending on the application. Refrigeration and cryocooling processes exploit the Joule–Thomson effect, by passing a gas through a valve or a throttling device [2]. The efficiency of compressors relies on the isentropic expansion coefficient μ_S of the refrigerant used, which should indeed not be too high [3]. Hydrocarbon mixtures and other fluids such as

* Corresponding author: dbroseta@univ-pau.fr

CO_2 rapidly flowing to or from an underground porous reservoir, and passing through the wellbore and pipelines and the numerous chokes and valves, experience rapid pressure variations that generate temperature changes. These changes may be so large that a second fluid phase, or even a solid phase (*e.g.*, hydrates [4] or paraffin [5, 6]) appears, leading to flow impairment [7]. Temperature well testing is another area where the knowledge of the JT coefficients helps interpret the data in terms of the composition of the produced fluids–gas, oil, or water [8]. Finally, it is worth mentioning here the recent surge in interest for the JT coefficients of CO_2-rich fluids in the context of CO_2 permanent storage in underground reservoirs. On the one hand, these coefficients play a role if CO_2 is injected in a depleted reservoir, because Joule–Thomson cooling may cause ice or hydrate formation and therefore severe injectivity problems [9]. On the other hand, the same effect provides a safety factor in case of CO_2 leakage from the reservoir, provided the temperature is low enough – below 10 °C, the maximum temperature of CO_2 hydrate stability – as is commonly encountered in offshore conditions [8, 10].

These coefficients are difficult to measure experimentally, and most often are estimated from an Equation of State (EoS) or from molecular simulations [11]. Kortekaas *et al.* [12] calculated the JT coefficients of North Sea gas condensates in the single-phase region using conventional cubic EoS. These calculations were however limited to conditions where the fluid forms a single-phase in the p–T domain investigated.

To date and the best of our knowledge, JT and isentropic expansion coefficients have been calculated for single-phase fluids only, except in the case of one-component fluids where simple closed-form expressions exist [12]. In the case of multi-component fluids, the calculations have been limited to the determination of the JTIC in the p–T plane, see *e.g.* Nichita and Leibovici [13] and Refs. [5, 6].

The purpose of this paper is to describe and implement on a few multi-component fluid examples simple calculation schemes based on an EoS for estimating the JT and isentropic expansion coefficients of fluids, both in the single- and two-phase domains. The multi-component fluids chosen are representative of geofluids – namely, hydrocarbon-rich fluids of underground reservoirs, some of them containing CO_2. One important expected feature is the discontinuity of these coefficients at the crossing of two-phase boundaries, which stems from the fact that these coefficients are related to first-order derivatives of state functions. This feature has been analyzed for one-component fluids by Sychev [14]. In this work, discontinuities for two-phase, multicomponent systems are calculated.

The paper is structured as follows. The next section is a brief reminder of how these two coefficients are related to each other and to other thermodynamic parameters, which are readily calculated from an EoS. The calculation procedure is outlined for a fluid system containing two phases in thermodynamic equilibrium. Examples are given for a variety of oils and gas condensates, *i.e.*, hydrocarbon mixtures exhibiting bubble or dew points, as well as a more complex fluid system. Conclusions are presented at the end of the paper. Three appendices give the expressions of

required thermodynamic functions calculated with an EoS, ideal gas heat capacities, and mixture compositions and component properties used in test examples.

2 The Joule–Thomson and isentropic expansion coefficients

The Joule–Thomson and isentropic expansion coefficients are related to the partial derivatives with respect to pressure p and temperature T of, respectively, the enthalpy H and entropy S of the fluid system by

$$\mu_{\mathrm{JT}} = \left(\frac{\partial T}{\partial p}\right)_H = -\left(\frac{\partial H}{\partial p}\right)_T \left(\frac{\partial H}{\partial T}\right)_p^{-1} \qquad (3)$$

and

$$\mu_S = \left(\frac{\partial T}{\partial p}\right)_S = -\left(\frac{\partial S}{\partial p}\right)_T \left(\frac{\partial S}{\partial T}\right)_p^{-1}. \qquad (4)$$

H and S also depend on the number of moles n_i of the various constituents $i = 1, \ldots, nc$, which are kept constant and for simplicity omitted in the above expressions. In the case of a multicomponent fluid system, with molar content $\boldsymbol{n} = (n_1, n_2, \ldots, n_{nc})$, the enthalpy and entropy are split into an ideal gas term, H^{ig} and S^{ig}, and a departure term directly related to the EoS, H^{dep} and S^{dep}

$$H = H^{\mathrm{ig}}(\boldsymbol{n}) + H^{\mathrm{dep}}(\boldsymbol{n}) \qquad (5)$$

and

$$S = S^{\mathrm{ig}}(\boldsymbol{n}) + S^{\mathrm{dep}}(\boldsymbol{n}). \qquad (6)$$

The above expressions (Eqs. (3)–(6)) hold when substituting H and S and their ideal and departure parts with their molar counterparts $h = H/n$, $s = S/n$, $h^{\mathrm{id}} = H^{\mathrm{id}}/n$, etc., where $n = n_1 + n_2 + \cdots + n_{nc}$ is the total number of moles. For cubic EoS, simple closed-form expressions exist for the departure parts $h^{\mathrm{dep}} = H^{\mathrm{dep}}/n$ and $s^{\mathrm{dep}} = S^{\mathrm{dep}}/n$ as a function of compositions or mole fractions, $z_i = n_i/n$. These expressions are given in Appendix A, for a general form of two-parameter cubic EoS, containing the Soave [15] and Peng-Robinson [16, 17] EoS. Note that any thermodynamic model can be used; only the expressions of enthalpy and entropy departures are required. On the other hand, the ideal parts $h^{\mathrm{id}} = H^{id}/n$ and $s^{\mathrm{id}} = S^{id}/n$ have partial derivatives with respect to temperature expressed as

$$\left(\frac{\partial h^{\mathrm{ig}}}{\partial T}\right)_n = \sum_{i=1}^{nc} z_i C_{\mathrm{pi}}(T) \qquad (7)$$

and

$$\left(\frac{\partial s^{\mathrm{ig}}}{\partial T}\right)_n = \sum_{i=1}^{nc} z_i \frac{C_{\mathrm{pi}}(T)}{T} \qquad (8)$$

where $C_{\mathrm{pi}}(T)$ is the ideal gas isobaric heat capacity per mole of component i (see Appendix B for the expressions

used in this work). The ideal gas enthalpy and entropy do not depend on pressure.

When two distinct phases (liquid and vapor, hereafter identified with subscripts L and V) are present, the enthalpy and entropy of the two-phase fluid system to consider in equations (3)–(6) are the sum of the enthalpies and entropies of the liquid and vapor phases, *i.e.*, $H_t = H_V + H_L$ and $S_t = S_V + S_L$ or, expressed on a molar basis:

$$h = h^{\mathrm{ig}}(\boldsymbol{z}) + \theta h_V^{\mathrm{dep}}(\boldsymbol{y}) + (1-\theta)h_L^{\mathrm{dep}}(\boldsymbol{x}) \qquad (9)$$

and

$$s = s^{\mathrm{ig}}(\boldsymbol{z}) + \theta s_V^{\mathrm{dep}}(\boldsymbol{y}) + (1-\theta)s_L^{\mathrm{dep}}(\boldsymbol{x}), \qquad (10)$$

where θ is the molar fraction of the vapor phase, and $\boldsymbol{x}$ and $\boldsymbol{y}$ are the vectors of liquid and vapor phase compositions, respectively (subscript t stands for total enthalpy and entropy). We assume in this work that thermodynamic equilibrium is ensured, which is legitimate when there are strong enough interdispersion and small domains of the two phases: these conditions hold for instance for a fluid in a porous medium, at least under incipient phase separation, i.e., near bubble or dew point conditions [1]. The quantities θ, $\boldsymbol{x}$, and $\boldsymbol{y}$ are then readily obtained from an EoS by a flash calculation for any given T and p. The partial derivatives of interest are obtained by numerical derivation of the enthalpy and entropy (whose expressions are given below for the ideal parts and in Appendix A for the departure part) along constant-pressure or constant-temperature paths around T and p.

The isobaric ideal gas heat capacity of one mole of the two-phase fluid is

$$C_p^{\mathrm{ig}} = \sum_{i=1}^{nc} z_i C_{\mathrm{pi}}^{\mathrm{ig}}(T). \qquad (11)$$

The ideal gas part of the molar enthalpy is

$$H^{\mathrm{ig}} = H_0^{\mathrm{ig}} + \sum_{i=1}^{nc} z_i \int_{T_0}^{T} C_p^{\mathrm{ig}}(T)\mathrm{d}T \qquad (12)$$

and the ideal part of entropy is

$$S^{\mathrm{ig}} = S_0^{\mathrm{ig}} + \sum_{i=1}^{nc} z_i \int_{T_0}^{T} \frac{C_p^{\mathrm{ig}}}{T}(T)\mathrm{d}T, \qquad (13)$$

where H_0^{ig} and S_0^{ig} are the ideal gas enthalpy and entropy at the reference conditions, respectively. These ideal parts depend only on temperature (not on pressure), hence the partial derivatives of the total enthalpy H_t with respect to pressure and temperature (see Eq. (3)) can be expressed as follows:

$$\left(\frac{\partial H_t}{\partial p}\right)_{T,\boldsymbol{n}} = \left(\frac{\partial H_L^{\mathrm{dep}}}{\partial p}\right)_{T,\boldsymbol{n}} + \left(\frac{\partial H_V^{\mathrm{dep}}}{\partial p}\right)_{T,\boldsymbol{n}} \qquad (14)$$

and

$$\left(\frac{\partial H_t}{\partial T}\right)_{p,\boldsymbol{n}} = \left(\frac{\partial H_L^{\mathrm{dep}}}{\partial T}\right)_{p,\boldsymbol{n}} + \left(\frac{\partial H_V^{\mathrm{dep}}}{\partial T}\right)_{p,\boldsymbol{n}} + \sum_{i=1}^{nc} z_i C_{\mathrm{pi}}. \quad (15)$$

Similarly, the partial derivatives of the total entropy S_t with respect to pressure and temperature (see Eq. (4)) are:

$$\left(\frac{\partial S_t}{\partial p}\right)_{T,\boldsymbol{n}} = \left(\frac{\partial S_L^{\mathrm{dep}}}{\partial p}\right)_{T,\boldsymbol{n}} + \left(\frac{\partial S_V^{\mathrm{dep}}}{\partial p}\right)_{T,\boldsymbol{n}} \qquad (16)$$

and

$$\left(\frac{\partial S_t}{\partial T}\right)_{p,\boldsymbol{n}} = \left(\frac{\partial S_L^{\mathrm{dep}}}{\partial T}\right)_{p,\boldsymbol{n}} + \left(\frac{\partial S_V^{\mathrm{dep}}}{\partial T}\right)_{p,\boldsymbol{n}} + \sum_{i=1}^{nc} z_i \frac{C_{\mathrm{pi}}}{T}. \quad (17)$$

Note that the partial derivatives with respect to pressure and temperature in equations (14)–(17) are at constant $\boldsymbol{n}$ (mixture composition). In this work, these derivatives are calculated numerically. An analytical treatment would require a framework similar to that presented in Ref. [13], relating the partial derivatives at constant $\boldsymbol{n}$ to those at constant $\boldsymbol{n}_k$ (phase compositions) obtained from the EoS, by differentiation of equations (A10) and (A11).

Another route to calculate the JT and isentropic expansion coefficients makes use of the differential expression of the enthalpy H

$$\mathrm{d}H = \mathrm{d}S + V\mathrm{d}p \qquad (18)$$

and the Maxwell relation

$$\left(\frac{\partial S}{\partial p}\right)_T = -\left(\frac{\partial V}{\partial T}\right)_p, \qquad (19)$$

leading to

$$\left(\frac{\partial H}{\partial p}\right)_T = T\left(\frac{\partial S}{\partial T}\right)_p + V \qquad (20)$$

and therefore, inserting equations (20) into (3) and equations (19) into (4),

$$\mu_{\mathrm{JT}} = \frac{1}{C_p}\left[T\left(\frac{\partial V}{\partial T}\right)_p - V\right] = \frac{V(T\alpha - 1)}{C_p}, \qquad (21)$$

$$\mu_S = \frac{1}{C_p}\left[T\left(\frac{\partial V}{\partial T}\right)_p\right] = \frac{VT\alpha}{C_p} \qquad (22)$$

where V is the volume and α is the isobaric thermal expansivity

$$\alpha = \frac{1}{V}\left(\frac{\partial V}{\partial T}\right)_p \qquad (23)$$

and

$$C_p = \left(\frac{\partial H}{\partial T}\right)_p = T\left(\frac{\partial S}{\partial T}\right)_p \qquad (24)$$

the isobaric heat capacity. The two coefficients are therefore related as follows:

$$\mu_{\mathrm{JT}} = \mu_S - \frac{V}{C_p}. \qquad (25)$$

Equations (21) and (22) are equivalent to equations (3) and (4), and offer an alternative route for estimating these coefficients. These equations hold at two-phase pressure and temperature conditions if the extensive thermodynamic functions involved are the sum of the contributions of the two equilibrium phases. When the fluid system contains two phases (liquid and vapor), the volume is the total volume

$$V_t = V_L + V_V = \frac{RT}{p}(n_L Z_L + n_V Z_V) \qquad (26)$$

with Z_L and Z_V the compressibility factors of the liquid and vapor phases (obtained from an EoS, see Appendix A, and a flash calculation), respectively. The two-phase expansivity and isobaric heat capacity are obtained by carrying out flash calculations at various temperatures near the temperature of interest along a constant pressure path.

The single-phase JTIC is calculated analytically, as detailed in Refs. [19, 20]. In the two-phase region, the location of the JTIC is calculated by tracking sign changes of the numerators (the denominators are always positive) in equations (3) or (21) on a given isotherm or isobar. Partial derivatives are calculated numerically by finite differences. It is incorrect to calculate the JTIC at feed composition in the two-phase domain.

3 Results and discussion

The single-phase and two-phase Joule–Thomson and isentropic expansion coefficients of several geofluids reported in the literature are calculated here with the Peng–Robinson EoS [16, 17] using the approaches described above. Some of the fluid examples and the pressure and temperature conditions chosen here are close to those considered in Ref. [13] where the focus was on the JTIC. The JT coefficients are therefore expected to be small, whether the fluid considered is an oil or a gas condensate at reservoir temperature (a few K/bar), much smaller than the typical values of gases at low pressure. All input data, that is, feed compositions z_i, component critical properties (temperature and pressure) acentric factors ω_i, molecular weights M_{Wi}, as well as Binary Interaction Parameters (BIPs) k_{ij} are taken from the literature. Riazi [21] and Kesler and Lee correlations [22] are used for the ideal gas isobaric heat capacity, for the light and heavy components, respectively. In the two-phase domain, the partial derivatives of enthalpy and entropy with respect to pressure and temperature are calculated numerically using a second-order central finite difference method (the pressure and temperature derivation steps used were $\Delta p = 0.0001$ bar and $\Delta T = 0.00001$ K, respectively; the sensitivity on the results to perturbations used in the numerical differentiation was carefully checked).

3.1 Reservoir fluid

The first example is the reservoir fluid (described by 20 components) studied by Stenby *et al.* [23]. The feed composition
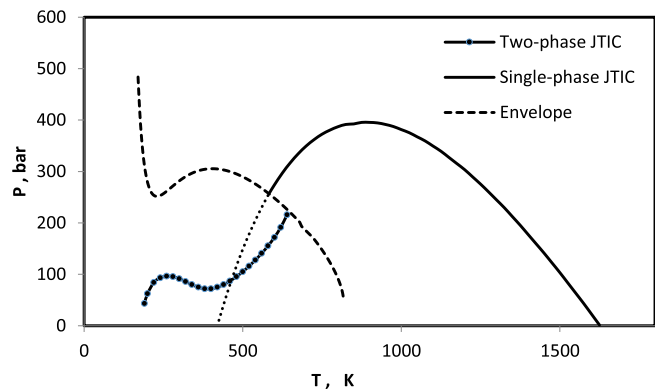

Figure 1. Joule–Thomson inversion curve and phase envelope of reservoir fluid (the dotted line indicates the extrapolation of the single-phase JTIC in the two-phase domain).

and component critical properties are taken from Nichita *et al.* [12] and are listed in Table C1. The non-zero BIPs in the EoS, taken also from Ref. [12] are: $k_{N_2-C_1} = 0.02$; $k_{N_2-C_2} = 0.06$; $k_{N_2-j \geq 5} = 0.08$; $k_{CO_2-C_1} = 0.12$; $k_{CO_2-j \geq 4} = 0.15$; $k_{C_1-C_6} = 0.0298$; $k_{C_1-C_7} = 0.035$; $k_{C_1-C_{11}} = 0.0442$; $k_{C_1-C_{14}} = 0.04488$; $k_{C_1-C_{16}} = 0.0512$; $k_{C_1-C_{20}} = 0.0544$; $k_{C_1-C_{23}} = 0.0565$; $k_{C_1-C_{27}} = 0.0586$; $k_{C_1-C_{32}} = 0.0609$; $k_{C_1-C_{38}} = 0.0627$; $k_{C_1-C_{48+}} = 0.08$.

The phase envelope and the JTIC are drawn in Figure 1. The JTIC exhibits three distinct branches: a branch in the single-phase region and an "S-shaped" branch in the two-phase region, which are connected by a segment of the bubble point curve. This allows up to three Joule–Thomson inversions on isotherms below the intersection of the two-phase branch with the phase boundary. The minimum inversion temperature located in the two-phase region is around 185 K and the maximum inversion temperature located in the single-phase region is about 1625 K. The variation of the Joule–Thomson coefficient in the P–T plane for temperatures from 225 K to 675 K and for pressures between 100 and 500 bar is depicted in Figure 2 (an arrow indicates the location of the phase boundary).

Figure 3 plots the reduced departure enthalpy H^{dep}/RT (note that the ideal part of the enthalpy does not depend on pressure) of this reservoir oil at four isotherms: $T = 400$ K, $T = 540$ K, $T = 615$ K, and $T = 650$ K, in the pressure interval from 100 to 400 bar. The Bubble Point (BP) pressures calculated with the PR EoS [16] for these isotherms are 305.4 bar, 275.65 bar, 240.28 bar, and 220.23 bar, respectively. The figure shows that the departure enthalpy exhibits angular points at the bubble point, *i.e.* a discontinuity of its derivative with respect to temperature. The single- and two-phase Joule–Thomson coefficients, calculated on the above isotherms in the pressure interval from 100 to 400 bar are plotted in Figure 4. The figure shows that the Joule–Thomson coefficient is negative at 400 K, it changes sign once at 540 and 650 K and three times at 615 K. The results agree with those from Ref. [12]. Except for the first isotherm where it varies in a monotonous manner, the Joule–Thomson coefficient exhibits discontinuities (corresponding to the angular points of the enthalpy in Fig. 3).
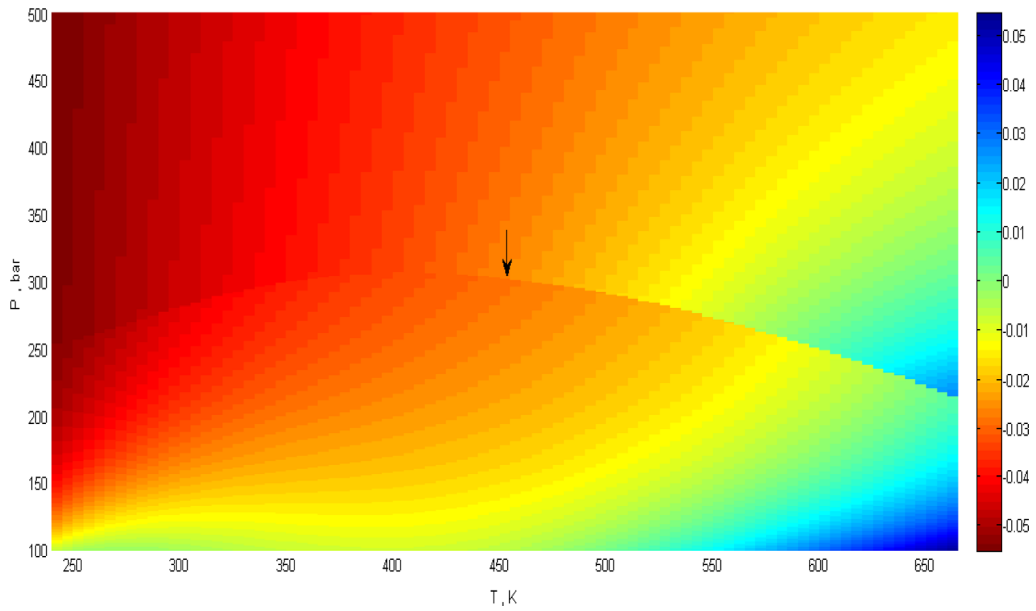
Figure 2. Joule–Thomson coefficient of the reservoir fluid in the intervals 225–675 K and 100–500 bar.
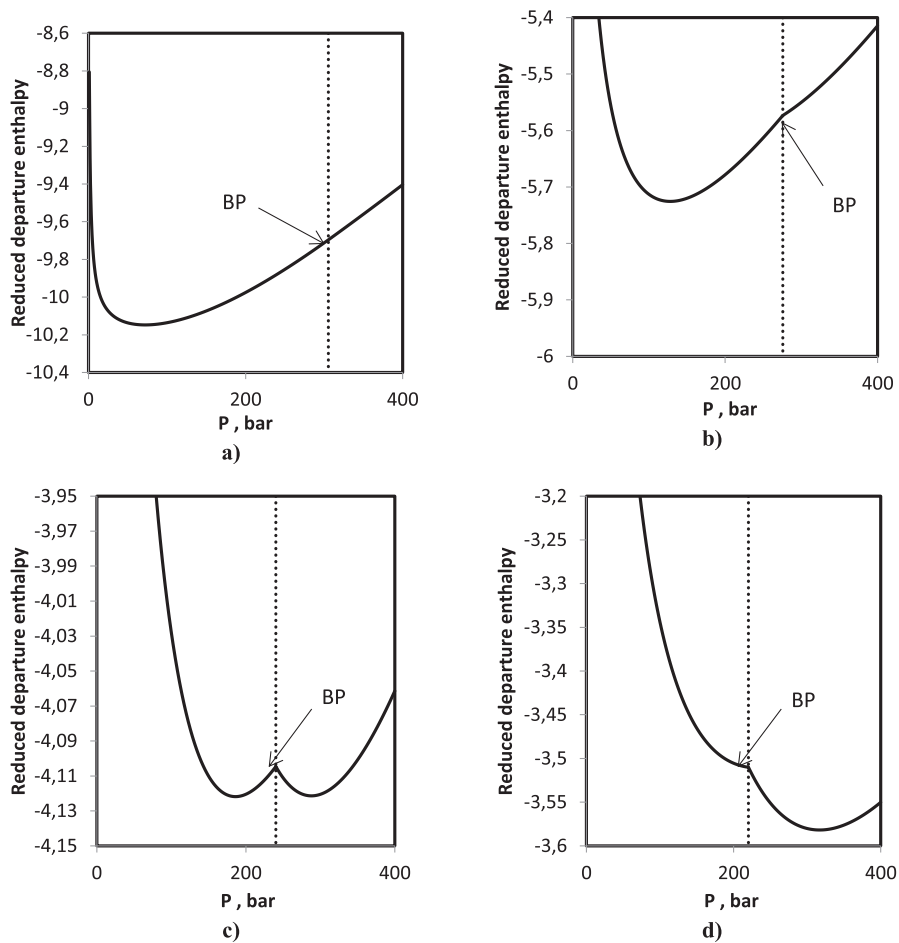

Figure 3. Reduced departure enthalpy of the reservoir fluid at: (a) $T = 400$ K, (b) $T = 540$ K, (c) $T = 615$ K and (d) $T = 650$ K.
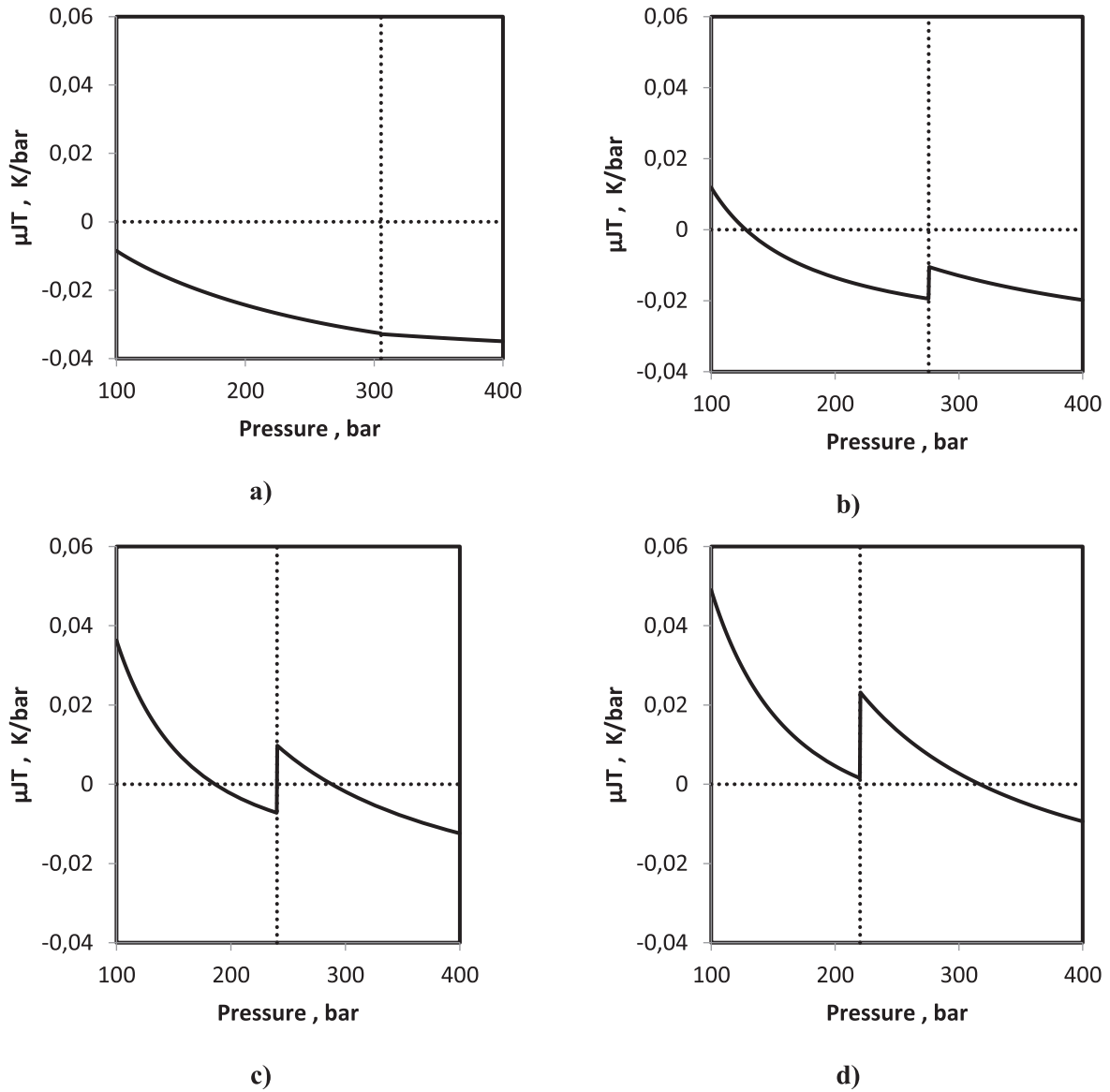
Figure 4. Joule–Thomson coefficient of reservoir fluid at: (a) $T = 400$ K, (b) $T = 540$ K, (c) $T = 615$ K and (d) $T = 650$ K.

The isentropic expansion coefficient of this reservoir fluid is represented in Figure 5 *vs.* pressure on four isotherms: $T = 400$ K, $T = 540$ K, $T = 615$ K, and $T = 650$ K, in the pressure interval from 100 to 400 bar. As expected, the isentropic expansion coefficient is positive at all four isotherms, therefore it presents no inversion. In a similar manner to the Joule–Thomson coefficient, the isentropic expansion coefficient varies in a monotonous manner, except at phase boundaries where it exhibits discontinuities (this corresponds to the angular points of the entropy variation with pressure).

3.2 North Sea gas condensate (Lille Frigg reservoir)

The second example is a 27-component North Sea (Lille Frigg reservoir) gas condensate in the temperature range from 300 to 500 K (the fluid system has no T_c), with feed composition, component properties taken from Nichita and Leibovici [13], see Table C2. The non-zero BIPs in the EoS are: $k_{N_2-CO_2} = 0.15$, $k_{N_2-j} = 0.12$, $k_{CO_2-j} = 0.15$, $k_{C_1-CN1} = 0.03$, $k_{C_1-CN2} = 0.05$ and $k_{C_2-CN2} = 0.03$.

The phase envelope and the JTIC are depicted in Figure 6. This mixture exhibits an open-shape phase envelope with no critical point. A dotted line indicated the extrapolation of the single-phase JTIC in the two-phase domain; it has no physical significance since the stable state of the mixture is a two-phase one and it is incorrect to calculate the JT inversion this way (as done for instance in Ref. [13]). There are three distinct branches of the JTIC: a single-phase branch, a portion of the dew point curve, and a two-phase branch. In a small temperature interval, there are three inversion pressures on a given isotherm. The variation of the Joule–Thomson coefficient in the P–T plane for
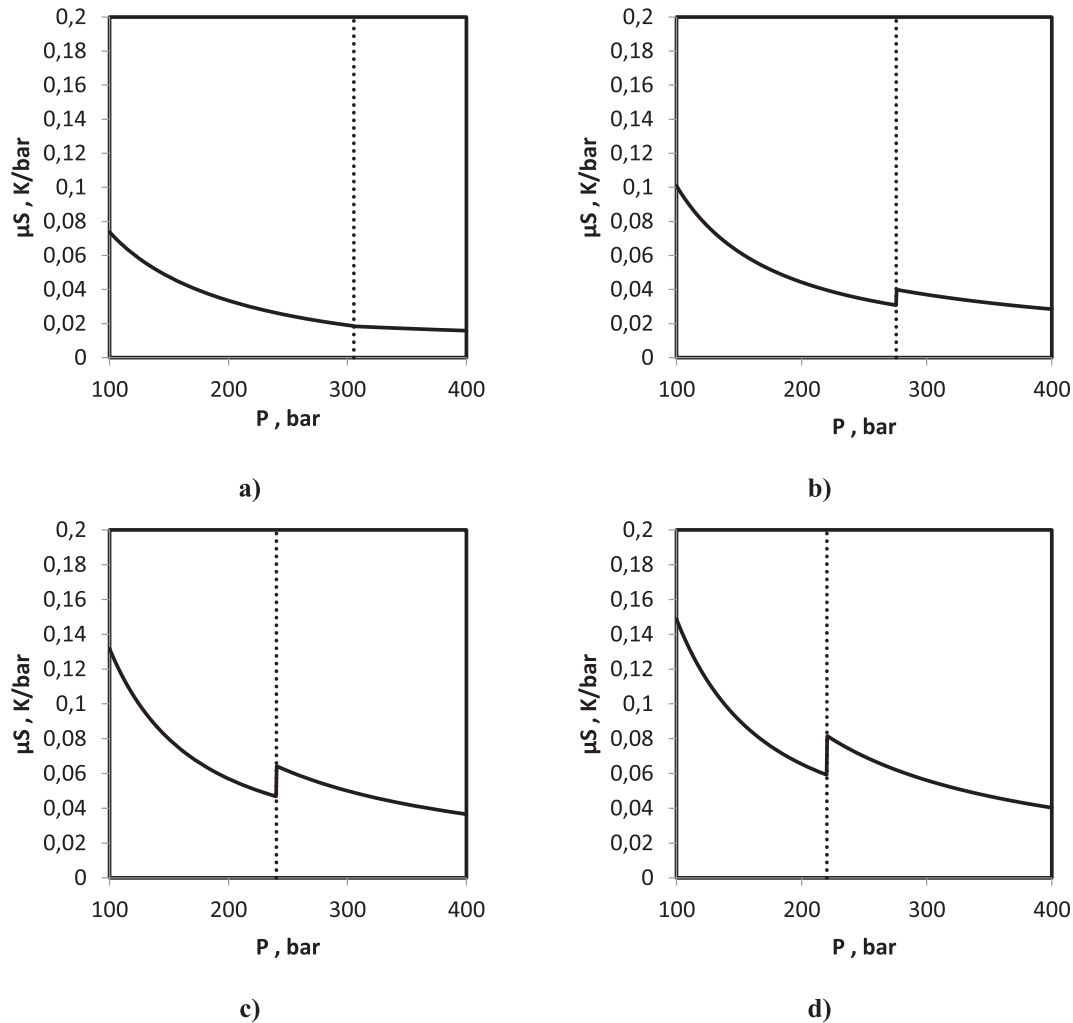
Figure 5. Isentropic expansion coefficient of reservoir fluid at: (a) $T = 400$ K, (b) $T = 540$ K, (c) $T = 615$ K and (d) $T = 650$ K.

a temperature range from 390 K to 470 K and a pressure range from 350 to 500 bar is drawn in Figure 7 (the location of the dew point curve is indicated by an arrow).

The reduced enthalpy departures of this mixture along three isotherms ($T = 400$ K, $T = 435$ K, and $T = 470$ K) are plotted in Figure 8 against pressure in the interval 400–600 bar. The dew-point pressures calculated with the PR EoS for the three isotherms are 545 bar, 495 bar, and 439 bar, respectively. The departure enthalpies exhibit angular points at dew-point pressures, corresponding to a discontinuity of their derivatives with respect to pressure. The results match those reported in Ref. [13].

The Joule–Thomson coefficients are plotted against pressure in Figure 9 for the above three isotherms in the pressure interval from 400 to 600 bar, with discontinuities at the phase boundary. At $T = 430$ K, Figure 9b shows three inversion pressures on this isotherm. The isentropic expansion coefficient is drawn *vs.* pressure for the same

three isotherms in Figure 10, exhibiting discontinuities at dew points; it is always positive with no inversion.

3.3 Bakken fluid

The third example, referred to as the Bakken fluid, is described by 8 components (four low-molecular-weight alkanes, two intermediate, and two heavy pseudo-components). The composition, component properties (given in Tab. C3) are taken from Nojabaei *et al.* [24]. The non-zero binary interaction parameters in the EoS are: $k_{1-2} = 0.005$, $k_{13} = k_{1-4} = 0.0035$, $k_{1-5} = 0.0035$, $k_{1-j \geq 6} = 0.0033$, $k_{2-3} = k_{2-4} = k_{2-5} = 0.0031$, $k_{2-j \geq 6} = 0.0026$.

The phase envelope and the JTIC calculated with the PR EoS are drawn in Figure 11 (the critical point coordinates are $T_c = 584.45$ K and $p_c = 259.25$ bar). The JTIC follows the bubble-point curve, from the intersection of the single-phase JTIC with the phase boundary towards low
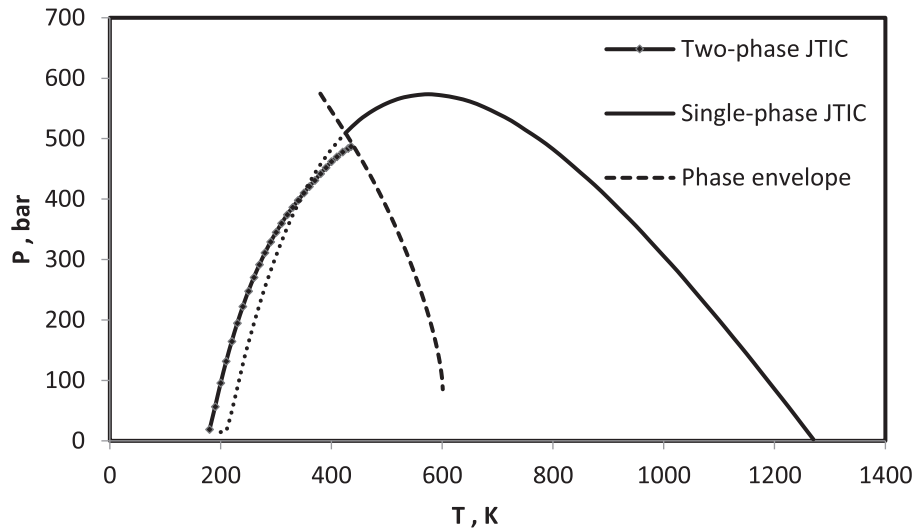
Figure 6. Joule–Thomson inversion curve and phase envelope of North-Sea gas condensate (the dotted line indicates the extrapolation of the single-phase JTIC in the two-phase domain).
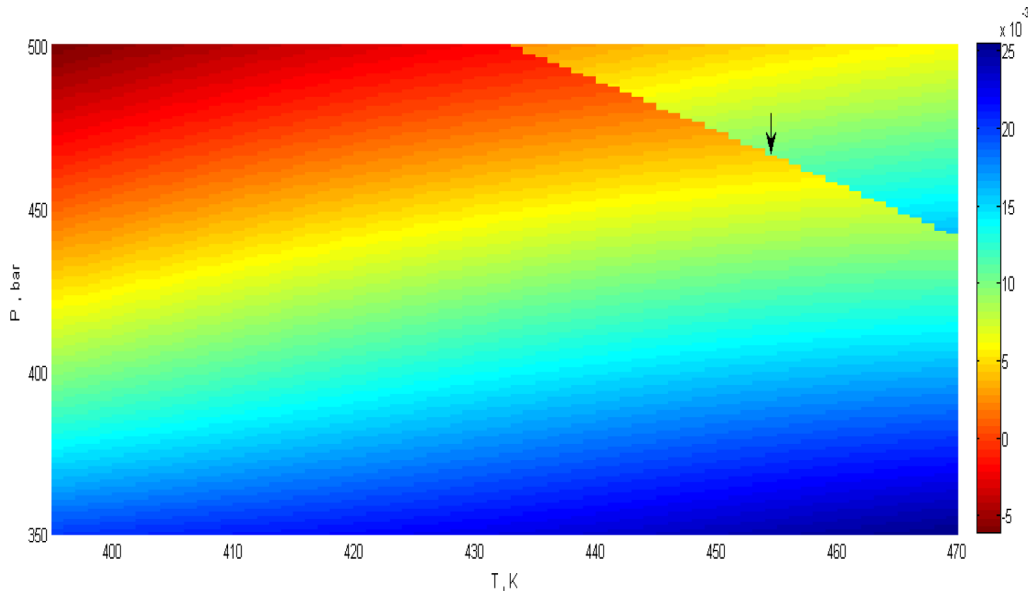

Figure 7. Joule–Thomson coefficient of the North Sea gas condensate in the intervals 390–470 K and 350–500 bar.

temperatures. This behavior is a reminiscence from pure fluids, for which the Joule–Thomson inversion takes place on the vapor pressure curve at low temperatures, as described earlier by Nichita and Leibovici [13] (see also Sychev [14]).

Figure 12 shows the variation of the Joule–Thomson coefficient in the P–T plane for temperatures from 200 K to 500 K and for pressures between 40 and 250 bar.

The calculations are carried out along the isotherm $T = 389.3$ K in the pressure interval from 100 to 400 bar, where the bubble point pressure is 197.69 bar. The results for the JT and isentropic expansion coefficients are depicted in Figures 13 and 14, respectively. When the pressure decreases along this isotherm and bubble point conditions are crossed, both coefficients experience a discontinuous

increase: in the case of the JT coefficient, the jump is from a negative to a positive value.

3.4 SJ15 fluid

The last example is a 15-component mixture, denoted here SJ15, with composition and component properties taken from Sherafati and Jessen [25] (listed in Tab. C4). The non-zero binary interaction parameters in the EoS are: $k_{N_2-CO_2} = 0.017$, $k_{N_2-C_1} = 0.0311$, $k_{N_2-C_2} = 0.0515$, $k_{N_2-C_3} = 0.0852$, $k_{N_2-iC_4} = 0.1033$, $k_{N_2-nC_4} = 0.0800$, $k_{N_2-iC_5} = 0.0922$, $k_{N_2-nC_5} = 0.10$, $k_{N_2-j\geq10} = 0.08$, $k_{CO_2-j\epsilon[29]} = 0.12$, $k_{CO_2-j>9} = 0.1$, $k_{C_1-PS1} = 0.028349$, $k_{C_1-PS2} = 0.044813$, $k_{C_1-PS3} = 0.062256$, $k_{C_1-PS4} = 0.077679$, $k_{C_1-PS5} = 0.0952$.
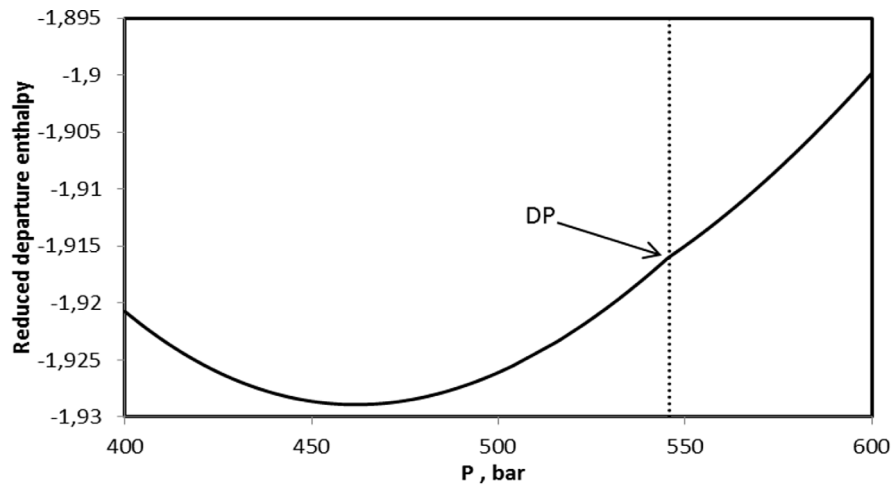
a)
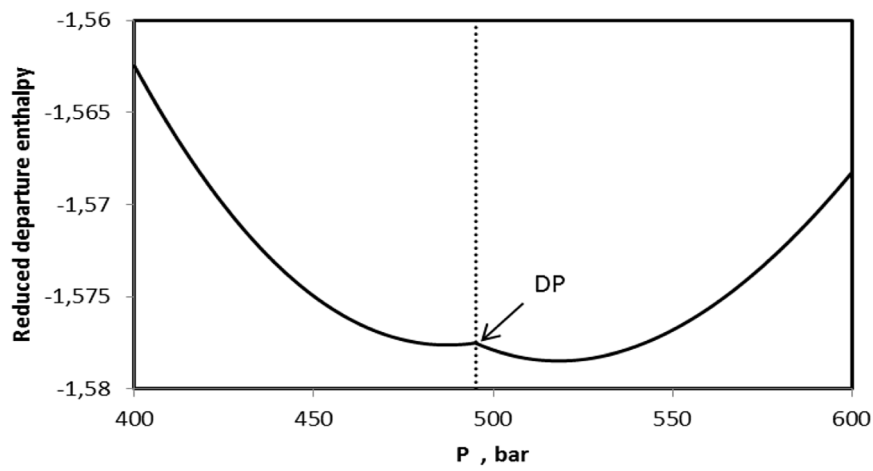
b)
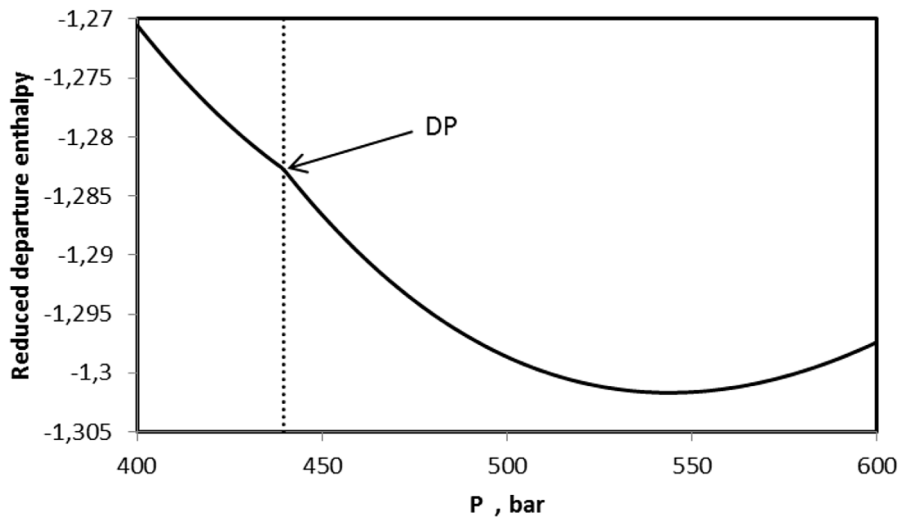
c)

Figure 8. Reduced departure enthalpy of North Sea gas condensate at: (a) $T = 400$ K, (b) $T = 430$ K and (c) $T = 470$ K.
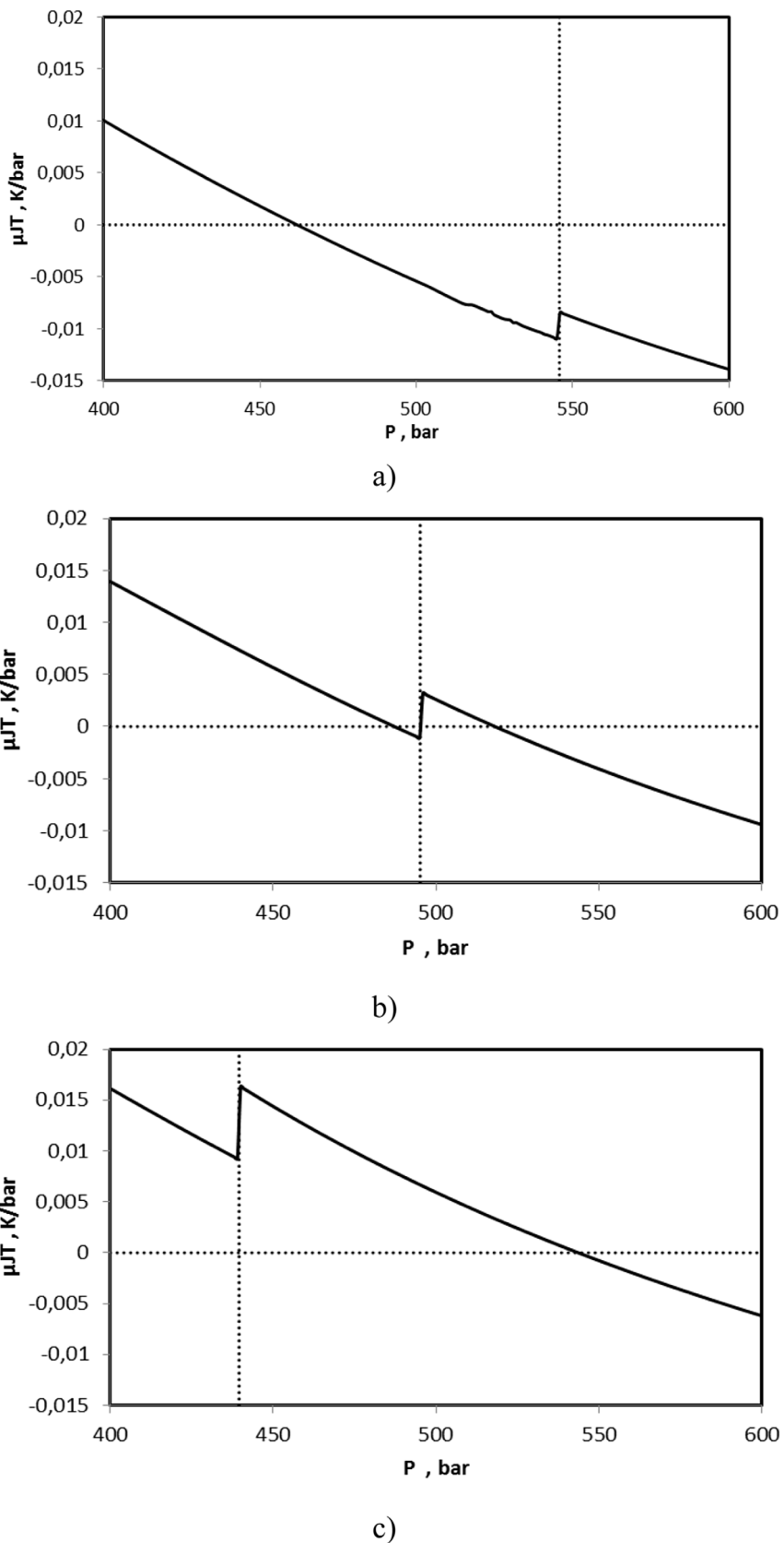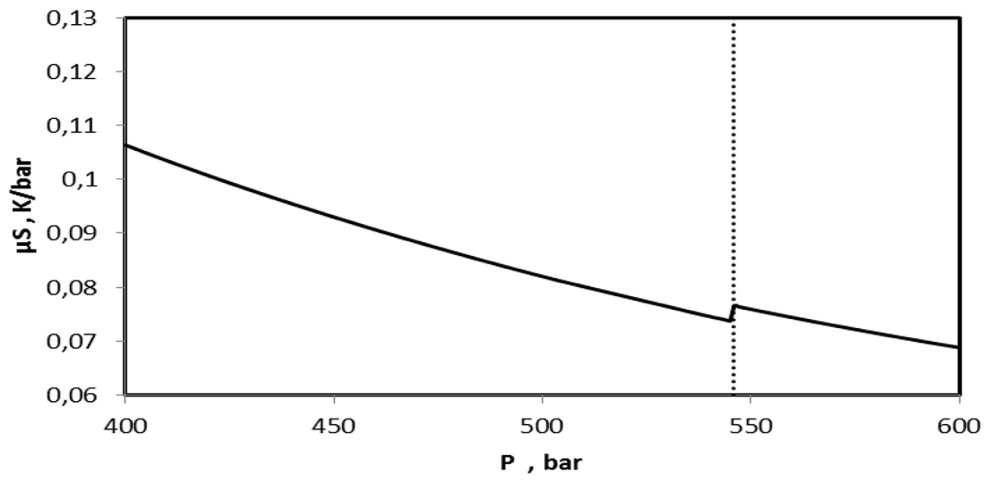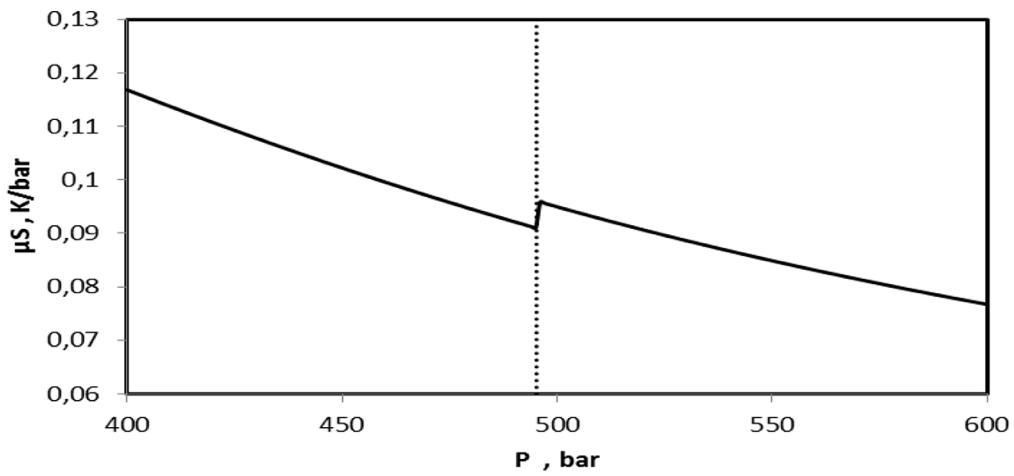
Figure 9. Joule–Thomson coefficient of the North Sea gas condensate at: (a) $T = 400$ K, (b) $T = 430$ K and (c) $T = 470$ K.

Figure 10. Isentropic expansion coefficient of the North Sea gas condensate at: (a) $T = 400$ K, (b) $T = 430$ K and (c) $T = 470$ K.
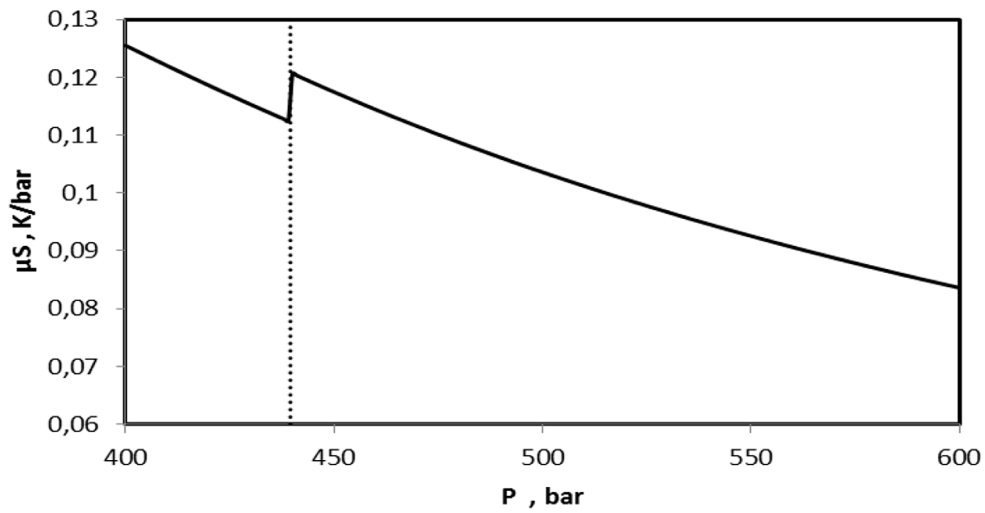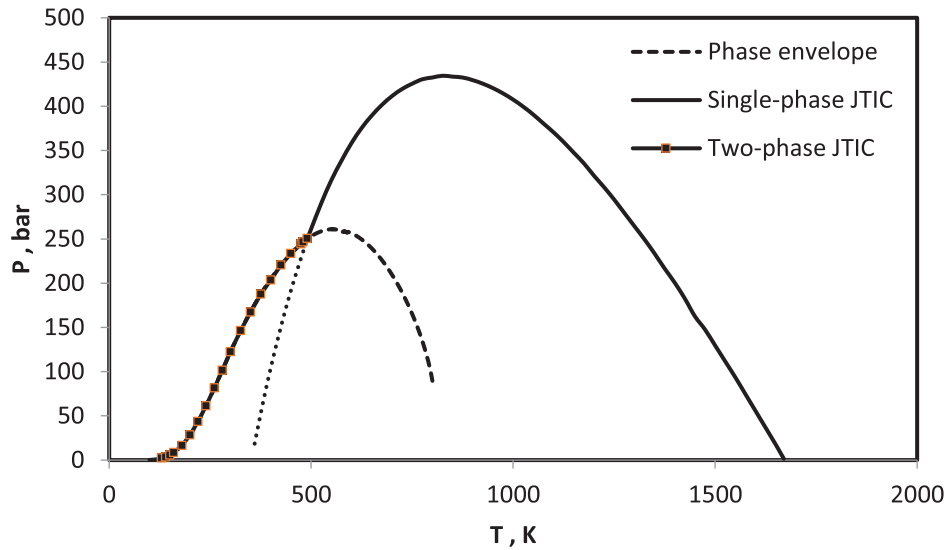
Figure 11. Joule–Thomson inversion curve and phase envelope of Bakken fluid (the dotted line indicates the extrapolation of the single-phase JTIC in the two-phase domain).
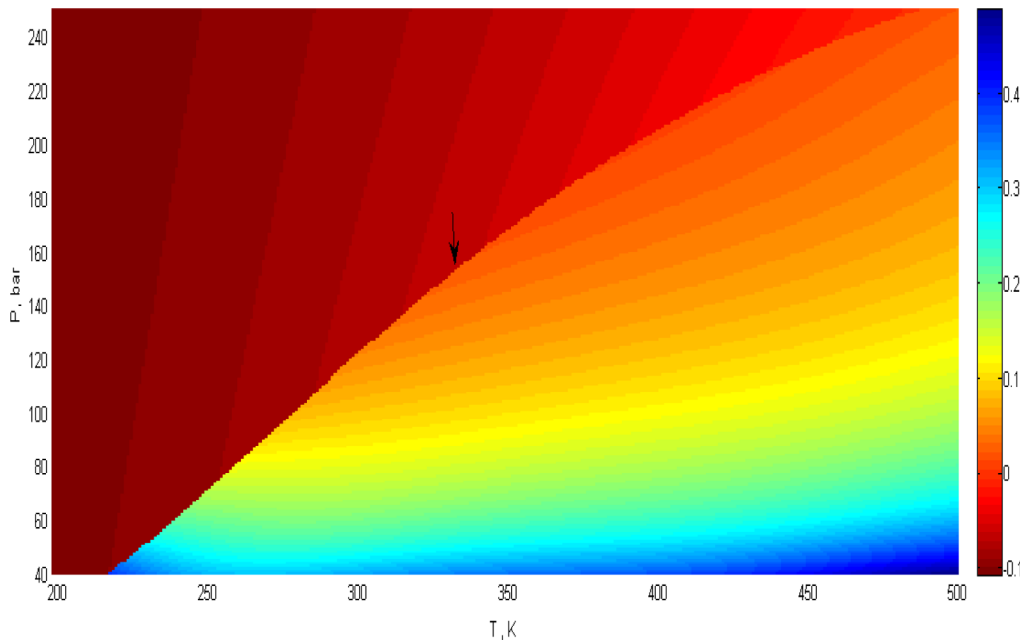

Figure 12. Joule–Thomson coefficient for the Bakken fluid in the intervals 200–500 K and 40–250 bar.

The phase envelope and the JTIC are plotted in Figure 15 (the critical point temperature is 721.34 K). The Joule–Thomson and isentropic expansion coefficients of the SJ15 fluid at $T = 383.15$ K in the pressure interval 50–200 bar are shown in Figures 16 and 17, respectively. These coefficients increase with decreasing pressure in a continuous manner, except at the bubble point pressure of 101.96 bar, where the JT coefficient jumps from a negative value in the single-phase (undersaturated liquid) region to a positive value in the two-phase liquid–vapor region. The isentropic expansion also experiences a similar jump but remains positive in the whole pressure interval.

4 Conclusions

We have defined and implemented two different but equivalent approaches to extend the calculation of both Joule–Thomson and isentropic expansion coefficients of
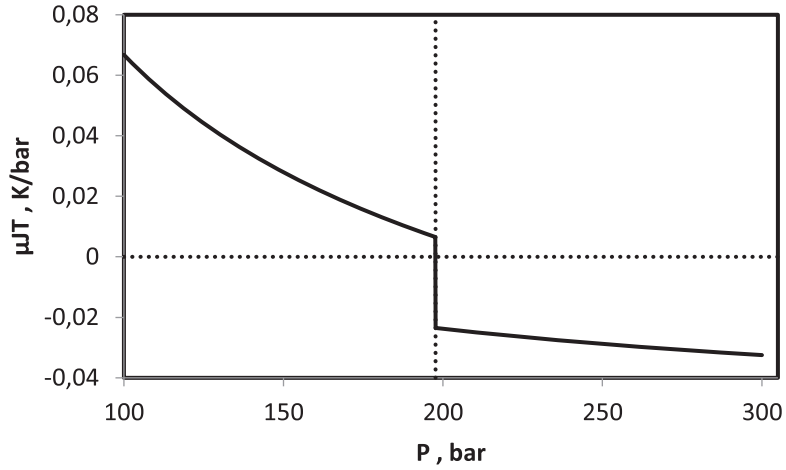
Figure 13. Joule–Thomson coefficient of Bakken fluid along the isotherm $T = 389.3$ K.
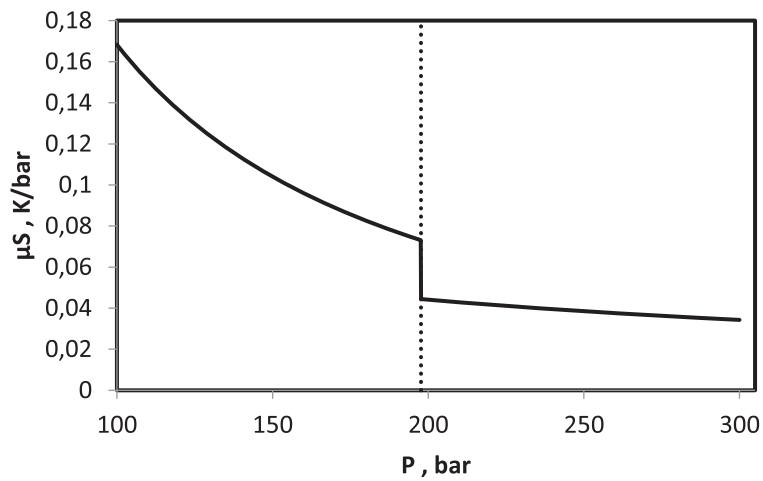
Figure 14. Isentropic expansion coefficient of Bakken fluid along the isotherm $T = 389.3$ K.
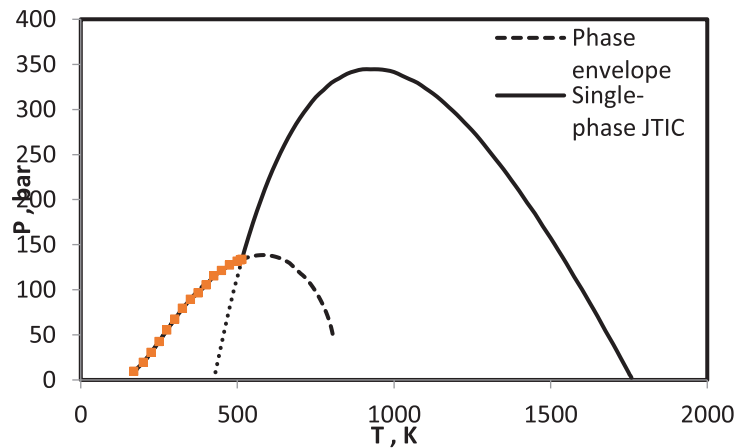
Figure 15. Joule–Thomson inversion curve and phase envelope of SJ15 fluid (the dotted line indicates the extrapolation of the single-phase JTIC in the two-phase domain).
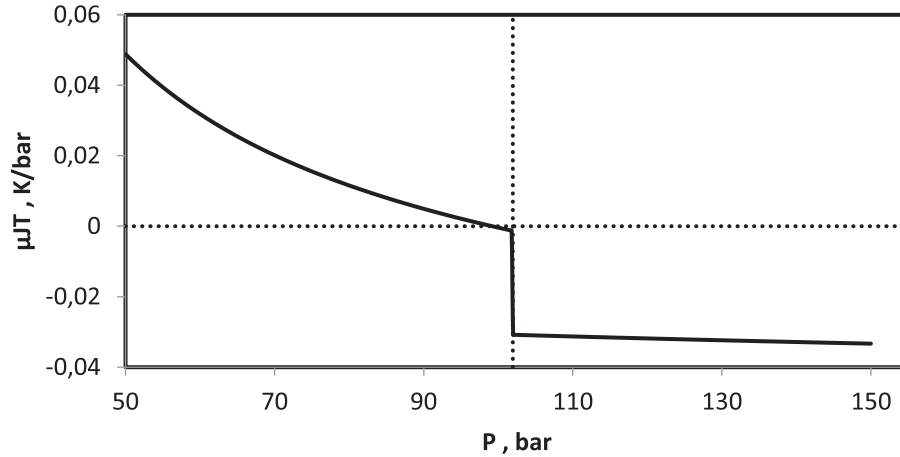
Figure 16. Joule–Thomson coefficient of SJ15 fluid along the isotherm $T = 383.15$ K.
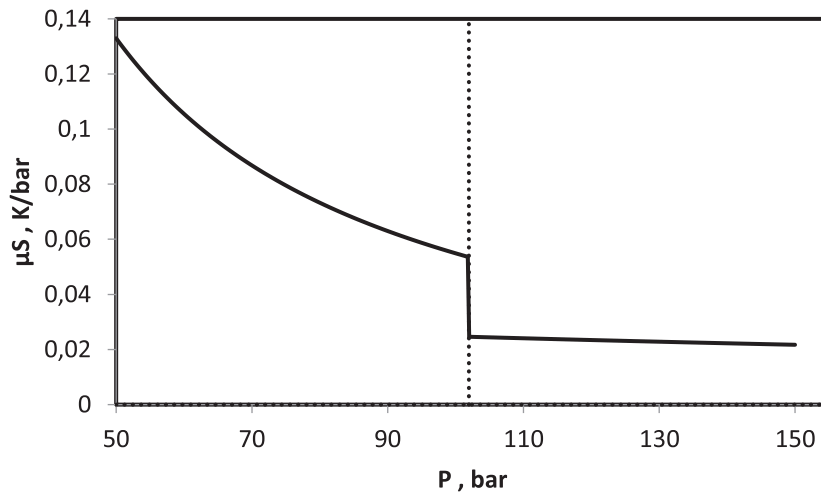

Figure 17. Isentropic expansion coefficient of SJ15 fluid along the isotherm $T = 383.15$ K.

fluid mixtures from the single-phase to the two-phase region. If one of these coefficients is known, the other can easily be obtained (by adding or subtracting $1/C_p$, where C_p is the total isobaric heat capacity at two-phase conditions). For both coefficients, a discontinuity occurs at liquid/vapor phase boundaries, which correspond to angular points of the enthalpy and entropy variations, respectively.

The JTIC may exhibit several branches: a branch in the single-phase region (down to the intersection with the phase boundary), a branch in the two-phase region, and a portion of the phase boundary itself. Thus, several inversion temperatures/pressures may occur at given pressure/temperature conditions. A rule seems to emerge from JTIC calculations for the test mixtures in this work and confirmed for many other mixtures (not reported here), that is, a two-phase branch exists for open-shaped (or S-shaped) phase envelopes). For closed-phase envelopes, the JT inversion takes place at the phase boundary at low temperatures, as a reminiscence from the behavior of pure fluids, where

the JT inversion takes place on the vapor pressure curve at low enough temperatures.

A cubic equation of state is used here, but any thermodynamic model can be used; beyond a two-phase flash calculation routine, only the expressions of the ideal part and of the residual (or departure) part (which is specific to a given EoS) of the enthalpy and entropy are required. In the two-phase region, the required partial derivatives can be calculated numerically, by a finite-difference scheme with the inputs obtained from flash calculations along a constant temperature or constant pressure path.

This work is a first step of a larger project, aimed to study the JT effect and other second-order derivative properties for CO_2 injection in depleted oil and gas reservoirs, as well as the difference between using conventional (at constant pressure and temperature) and isobar-isenthalpic phase equilibrium calculations in compositional reservoir simulation. From practical reasons, in hydrocarbons-brine-CO_2 systems, it is sufficient to use a robust multiphase flash routine and an accurate evaluation of enthalpies in the

multiphase region; an accurate equation of state must be used for the aqueous phase and an adapted thermodynamic model is required to account for salinity.

References

1 Anderson A.C., Reese W., Wheatley J.C. (1963) Specific heat, entropy, and expansion coefficient of liquid helium 3, *Phys. Rev.* **130**, 495–501.

2 Alabdulkarem A., Hwang Y., Radermacher R. (2012) Development of CO_2 liquefaction cycles for CO_2 sequestration, *Appl. Therm. Eng.* **33**, 144–156.

3 Maytal B.Z., Pfotenhauer J.M. (2013) Miniature Joule–Thomson cryocooling, in: *Principles and Practice, International Cryogenics Monograph Series*, Springer.

4 Ullrich A., Eggers R. (2004) Hydrate formation during pressure release of wet CO_2, view-cell observations, *Chem. Eng. Technol.* **27**, 583–588.

5 Nichita D.V., Bessieres D., Daridon J.L. (2008) Calculation of Joule–Thomson inversion curves for multiphase systems with waxy solid-phase precipitation, *Energy Fuels* **22**, 4012–4018.

6 Nichita D.V., Pauly J., Daridon J.L. (2009) Joule–Thomson inversion in vapor–liquid–solid solution systems, *Int. J. Thermophys.* **30**, 1130–1143.

7 Thirumaleshwar M., Richardson R.N. (1994) Enhancement of J–T cooling using multi-component mixtures, *Cryogenics* **34**, 123–125.

8 Oldenburg C.M. (2007) Joule–Thomson cooling due to CO_2 injection into natural gas reservoirs, *Energy Convers. Manag.* **48**, 1808–1815.

9 Mathias S.A., McElwaine J.N., Gluyas J.G. (2014) Heat transport and pressure buildup during carbon dioxide injection into depleted gas reservoirs, *J. Fluid Mech.* **756**, 89–109.

10 Gauteplass J., Almenningen S., Ersland G., Barth T. (2018) Hydrate seal formation during laboratory CO_2 injection in a cold aquifer, *Int. J. Greenh. Gas Control* **78**, 21–26.

11 Lagache M., Ungerer P., Boutin A., Fuchs A.H. (2001) Prediction of thermodynamic derivative properties of fluids by Monte Carlo simulation, *Phys. Chem. Chem. Phys.* **3**, 4333–4339.

12 Kortekaas W.G., Peters C.J., de Swaan Arons J. (1997) Joule–Thomson expansion of high-pressure-high-temperature gas condensates, *Fluid Phase Equilib.* **139**, 205–218.

13 Nichita D.V., Leibovici C.F. (2006) Calculation of Joule–Thomson inversion curves for two-phase mixtures, *Fluid Phase Equilib.* **246**, 167–176.

14 Sychev V.V. (1983) *The differential equations of thermodynamics*, MIR Editions.

15 Soave G. (1972) Equilibrium constants from a modified Redlich–Kwong equation of state, *Chem. Eng. Sci.* **27**, 1197–1203.

16 Peng D.Y., Robinson D.B. (1976) A new two-constant equation of state, *Ind. Eng. Chem. Fund.* **15**, 59–64.

17 Robinson D.B., Peng D.Y. (1978) *The characterization of the heptanes and heavier fractions for the GPA Peng-Robinson programs, Research Report RR-28*, Gas Processors Association.

18 Nichita D.V., Khalid P., Broseta D. (2010) Calculation of isentropic compressibility and sound velocity in two-phase fluids, *Fluid Phase Equilib.* **291**, 95–102.

19 Leibovici C.F., Nichita D.V. (2007) Parametric generation of single-phase properties (PT curves) for most cubic equations of state and any mixing rules, *Chem. Eng. Commun.* **194**, 648–655.

20 Nichita D.V., Leibovici C.F. (2011) Parametric construction of characteristic curves, *Fluid Phase Equilib.* **300**, 83–88.

21 Riazi M.R. (2005) *Characterization and properties of petroleum fractions*, 1st edn., Vol. **50**, ASTM International, Philadelphia, PA, pp. 242, 246.

22 Kesler M.G., Lee B.I. (1976) Improved prediction of enthalpy of fractions, *Hydrocarb. Process.* **55**, 153–158.

23 Stenby E.H., Christensen J.R., Knudsen K., Leibovici C. (1996) Application of a delumping procedure to compositional reservoir simulations, SPE-36744-MS, SPE Annual, Technical Conference and Exhibition, October 1996, Denver, Colorado. https://doi.org/10.2118/36744-MS.

24 Nojabaei B., Johns R.T., Chu L. (2013) Effect of capillary pressure on phase behavior in tight rocks and shales, *SPE Res. Eval. Eng.* **16**, 281–289.

25 Sherafati M., Jessen K. (2017) Stability analysis for multi-component mixtures including capillary pressure, *Fluid Phase Equilib.* **433**, 56–66.

26 Riazi M.R., Al-Sahhaf T.A. (1996) Physical properties of heavy petroleum fractions and crude oils, *Fluid Phase Equilib.* **117**, 217–224.

Appendix A

A general form of two-parameter cubic EoS is used in this work. Its explicit in pressure form is

$$P = \frac{nRT}{V - bn} - \frac{an^2}{(V + \delta_1 bn)(V + \delta_2 bn)}, \qquad (A1)$$

where $\delta_{1,2} = 1 \pm \sqrt{2}$ for the Peng–Robinson (PR) EoS [16, 17] and $\delta_1 = 1$, $\delta_2 = 0$ for the Soave–Redlich–Kwong (SRK) EoS [15].

The van der Waals mixing rules are used for the energy, a for the volume and b parameters of the EoS

$$a = \sum_{i=1}^{nc} \sum_{j=1}^{nc} x_i x_j \sqrt{a_i} \sqrt{a_j} \left(1 - k_{ij}\right), \qquad (A2)$$

$$b = \sum_{j=1}^{nc} x_j b_j, \qquad (A3)$$

where

$$a_i = \Omega_a \frac{R^2 T_{ci}^2}{p_{ci}} \left[1 + m(\omega_i)\left(1 - \sqrt{\frac{T}{T_{ci}}}\right)\right]^2, \qquad (A4)$$

$$b_i = \Omega_b \frac{R T_{ci}}{p_{ci}}, \qquad (A5)$$

in which k_{ij} is the Binary Interaction Parameter (BIP) between components i and j.

The values of Ω_a and Ω_b and the expression of the function $m(\omega_i)$ are specific to a given EoS. For the PR EoS $\Omega_a = 0.45724$, $\Omega_a = 0.0778$ and $m(\omega_i)$ is [15, 16]

$$m(\omega) = 0.37464 + 1.54226\omega - 0.26992\omega^2;$$
$$\omega < 0.49, \tag{A6}$$

$$m(\omega) = 0.379642 + 1.48503\omega - 0.164423\omega^2 + 0.016667\omega^3;$$
$$\omega \geq 0.49.$$

For the SRK EoS, $\Omega_a = 0.42748$, $\Omega_b = 0.08664$ [14] and

$$m(\omega) = 0.48508 + 1.55171\omega - 0.15613\omega^2. \tag{A7}$$

The implicit form (in compressibility factor Z) of the EoS is obtained by substituting $A = ap/R^2T^2$, $B = bp/RT$, and $Z = pv/RT$ into equation (A1)

$$Z^3 + [(\delta_1 + \delta_2 - 1)B - 1]Z^2$$
$$+ [A + \delta_1\delta_2 B^2 - (\delta_1 + \delta_2)B(B+1)]Z$$
$$- [AB + \delta_1\delta_2 B^2(B+1)] = 0. \tag{A8}$$

The fugacity coefficients are, for $i = 1$, nc and $k = V$, L

$$\ln\varphi_{ik} = (Z_k - 1)\frac{B_i}{B_k} - \ln(Z_k - B_k)$$
$$- \frac{1}{(\delta_1 - \delta_2)B_k}\left(2\sum_{j=1}^{nc} x_j A_{ij} - A_k\frac{B_i}{B_k}\right)\ln\left(\frac{Z_k + \delta_1 B_k}{Z_k + \delta_2 B_k}\right). \tag{A9}$$

From the general form of the cubic equations of state, h_k^{dep} is expressed as follows:

$$h_k^{\mathrm{dep}} = RT\left\{Z_k - 1 - \frac{1}{(\delta_1 - \delta_2)b_k RT}\left[a_k - T\frac{\mathrm{d}a_k}{\mathrm{d}T}\right]\ln\left(\frac{Z_k + \delta_1 B_k}{Z_k + \delta_2 bB_k}\right)\right\} \tag{A10}$$

and s_k^{dep} is

$$s_k^{\mathrm{dep}} = -R\left[\ln\left(\frac{p}{p_0}\right) - \ln(Z_k - B_k) - \frac{\frac{\mathrm{d}a_k}{\mathrm{d}T}}{(\delta_1 - \delta_2)b_k R}\right.$$
$$\left.\ln\left(\frac{Z_k + \delta_1 B_k}{Z_k + \delta_2 B_k}\right) + \sum_{i=1}^{nc} x_{ik}\ln(x_{ik})\right], \tag{A11}$$

where p_0 is the reference pressure (taken equal to 1 bar).

Appendix B

The ideal gas isobaric heat capacity $C_p(T)$ for one mole of light hydrocarbon components (specific carbon number less than 7) and non-hydrocarbon components is calculated with the correlation of Riazi [21], which consists in a four degree polynomial function in temperature

$$C_p(T) = C_{p,0} + C_{p,1}T + C_{p,2}T^2 + C_{p,3}T^3 + C_{p,4}T^4. \tag{B1}$$

The constants $C_{p,i}$, $i = 0$, 4 are tabulated in Ref. [20].

Kesler and Lee [21] give the constants $C_{p,i}$, $i = 0$, 2 for a single heavy hydrocarbon fraction (specific carbon number greater than 7), as follows:

$$C_{p,0} = -0.33886 + 0.02827K_w - 0.06105CF + 0.59332\omega CF,$$

$$C_{p,1} = [-0.9291 + 1.1543K_w - 0.0368K_w^2$$
$$+ CF(4.56 - 9.48\omega)]10^{-4},$$

$$C_{p,2} = -1.6659 * 10^{-7} + CF(0.536 - 0.6828\,\omega)10^{-7},$$

$$C_{p,3} = C_{p,4} = 0,$$

where

$$CF = [(12.8 - K_w)(10 - K_w)/(10\omega)]^2$$

ω and K_w are respectively, the acentric factor and Watson factor:

$$K_w = 4.5579M_W^{0.15178}\mathrm{SG}^{-0.84573}, \tag{B2}$$

where M_W (in g/mol) and SG are the molar weight and the specific gravity, respectively. In this correlation, the temperature is in Rankin (°R) and C_p in Btu·Ib^{-1}°F^{-1} unit (1 Btu·Ib^{-1}°F^{-1} = 4.187 KJ/(Kg·K)).

The specific gravity is obtained from the Riazi and Al-Sahhaf correlation [25] (valid from C_6 to C_{50})

$$\mathrm{SG} = 1.07 - \exp\left(3.56073 - 2.93886M_W^{0.1}\right). \tag{B3}$$

Appendix C

Table C1. Feed composition, component critical properties, and molar weight of reservoir fluid.

nc°	Comp.	z_i	T_c [K]	p_c [bar]	ω [–]	M_W [g/mol]
1	N_2	0.00403	126.20	33.60	0.04	28.01
2	CO_2	0.01000	304.20	72.90	0.23	44.01
3	C_1	0.45396	190.60	45.40	0.01	16.04
4	C_2	0.04202	305.40	48.20	0.10	30.07
5	C_3	0.00887	369.80	41.90	0.15	44.09
6	iC_4	0.00561	408.10	36.00	0.18	58.12
7	nC_4	0.00518	425.20	37.50	0.19	58.12
8	iC_5	0.00647	460.40	33.40	0.23	72.15
9	nC_5	0.00294	469.60	33.30	0.25	72.15
10	C_6	0.01011	507.40	29.30	0.30	86.18
11	C_7	0.13117	567.16	29.01	0.52	111.89
12	C_{11}	0.07127	633.70	21.51	0.66	163.22
13	C_{14}	0.03847	671.11	18.92	0.75	198.71
14	C_{16}	0.06005	710.30	17.18	0.85	239.54
15	C_{20}	0.03352	752.38	15.90	0.96	289.22
16	C_{23}	0.03340	790.47	15.14	1.06	337.54
17	C_{27}	0.02870	835.97	14.54	1.17	399.66
18	C_{32}	0.02179	887.86	14.12	1.27	475.59
19	C_{38}	0.01892	956.19	13.85	1.35	581.43
20	C_{48+}	0.01351	1090.01	13.80	1.24	797.11

Table C2. Feed composition, component critical properties, and molar weight of North Sea gas condensate.

nc°	Comp.	z_i	T_c [K]	p_c [bar]	ω [–]	M_W [g/mol]
1	CO_2	0.019549	304.20	73.77	0.2250	44.01
2	N_2	0.003243	126.20	33.94	0.0400	28.01
3	C_1	0.761530	190.60	46.00	0.0115	16.04
4	C_2	0.077367	305.40	48.84	0.0908	30.07
5	C_3	0.036177	369.80	42.45	0.1454	44.10
6	iC_4	0.005667	408.10	36.48	0.1750	58.12
7	nC_4	0.013258	425.20	38.00	0.1928	58.12
8	iC_5	0.004480	460.26	33.83	0.2271	72.15
9	nC_5	0.006100	469.60	33.74	0.2273	72.15
10	CC5	0.000580	511.60	45.09	0.1923	70.14
11	PC6	0.006001	503.79	30.07	0.2860	86.18
12	CC6	0.004148	547.41	39.90	0.2215	84.16
13	AC7	0.001735	562.10	48.94	0.2100	78.11
14	PC7	0.004239	536.44	27.60	0.3364	100.21
15	CC7	0.005056	566.27	34.69	0.2451	98.19
16	AC7	0.003063	591.70	41.14	0.2566	92.14
17	PC8	0.003291	565.05	25.02	0.3816	114.23
18	CC8	0.002540	594.05	29.74	0.2391	112.21
19	AC8	0.002564	619.46	35.84	0.3228	106.16
20	PC9	0.002630	590.64	23.29	0.4230	128.25
21	CC9	0.001640	621.21	28.39	0.2998	125.97
22	AC9	0.001217	644.06	32.08	0.3725	120.16
23	PC10	0.002411	613.72	21.46	0.4646	142.28
24	CC10	0.000427	621.58	26.25	0.4058	140.20
25	AC10	0.001049	670.83	29.72	0.3642	133.80
26	CN-1	0.026703	711.04	18.75	0.8000	240.00
27	CN-2	0.003338	848.08	16.33	1.3000	450.26

Table C3. Feed composition, component critical properties, and molar weight of Bakken fluid.

nc°	Comp.	z_i	T_c [K]	p_c [bar]	ω [–]	M_W [g/mol]
1	C_1	0.36736	186.297778	45.1620373	0.0102	16.535
2	C_2	0.14885	305.538333	49.7794561	0.1028	30.433
3	C_3	0.09334	369.983333	42.4551557	0.1520	44.097
4	C_4	0.05751	421.782222	37.6770891	0.1894	58.124
5	C_5–C_6	0.06406	486.377222	31.8048246	0.2684	78.295
6	C_7–C_{12}	0.15854	585.138889	25.0514101	0.4291	120.562
7	C_{13}–C_{21}	0.07330	740.052778	17.210003	0.7203	220.716
8	C_{22}–C_{80}	0.03704	1024.71722	13.108312	1.0159	443.518

Table C4. Feed composition, component critical properties, and molar weight of SJ15 fluid.

Comp.	z_i	T_c [K]	p_c [bar]	ω [–]	M_W [g/mol]
N_2	0.0018	126.20	34.045200	0.040	28.016
CO_2	0.0082	304.20	73.865925	0.228	44.010
C_1	0.2292	190.60	46.001550	0.008	16.043
C_2	0.0721	305.40	48.838650	0.098	30.069
C_3	0.0737	369.80	42.455175	0.152	44.096
iC_4	0.0158	408.10	36.477000	0.176	58.123
nC_4	0.0523	425.20	37.996875	0.193	58.123
iC_5	0.0225	460.40	33.842550	0.227	72.150
nC_5	0.0360	469.60	33.741225	0.251	72.150
C_6	0.0484	507.60	29.688225	0.296	86.177
PS1	0.196107	565.85	29.708490	0.34612	120.312
PS2	0.113893	683.44	20.102880	0.57838	207.159
PS3	0.066598	798.99	13.3242375	0.90175	354.274
PS4	0.041047	899.68	9.6968025	1.19183	574.812
PS5	0.022355	1013.31	7.6703025	1.39383	1055.440